Hydrogen storage by adsorption on activated carbon: Investigation of the thermal effects during the charging process

G. Hermosilla-Lara[a,b,*], G. Momen[a], P.H. Marty[b], B. Le Neindre[a], K. Hassouni[a]

[a]*Laboratoire d'Ingénierie des Matériaux et des Hautes Pressions, CNRS UPR 1311-Université Paris 13, 93430 Villetaneuse, France*
[b]*Laboratoire des Ecoulements Géophysiques et Industriels, BP 53, 38041 Grenoble Cedex 9, France*

Available online 18 December 2006

Abstract

This paper presents an investigation of the thermal effects during high-pressure charging of a packed bed hydrogen storage tank. The studied column is packed with activated IRH3 carbon, which has an average surface area of $2600 \, m^2 \, g^{-1}$ and is fed with hydrogen or helium from an external high-pressure source. The temperature at six locations in the storage tank and the pressure value at the bottom of the tank are recorded during the charging stage. Several experiments were carried out to investigate the effect of the initial flow rate on the temperature field in the reservoir and on the duration of the charging process. A study of the respective contribution of adsorption and mechanical dissipation effects to the thermal phenomena is done in the case of hydrogen. Experimental results are compared to those obtained with the commercial code Fluent. A fair agreement is found when comparing typical pressure and temperature evolutions during the tank filling.
© 2006 International Association for Hydrogen Energy. Published by Elsevier Ltd. All rights reserved.

Keywords: Adsorption; Hydrogen storage; Thermal effects; Numerical simulation

1. Introduction

Aside from many other applications, hydrogen is an advantageous energy source because it is renewable and its use would reduce the emission of pollution. It has been considered as an ideal energy medium for replacing fossil fuels such as oil and coal. An electrical vehicle powered by a hydrogen fuel cell will require 3.1 kg of hydrogen to achieve a range of 500 km. This amount, when stored in a typical gasoline tank, would correspond to a hydrogen density of $65 \, kg \, m^{-3}$ and 6.5 wt% of the whole storage system [1]. Presently, only liquid hydrogen (LH$_2$) systems (with a density of $51 \, kg \, m^{-3}$ and 14 wt%) is close to this target. However, the cost of LH$_2$ as a transportation fuel is nearly twice that of gaseous hydrogen (GH$_2$), due to the liquefaction process, increased fuel transportation costs and more complex manipulation of the fuel. The challenge is how

to transport and store hydrogen safely and efficiently. There are four main methods for hydrogen storage. These are liquid hydrogen, compressed hydrogen, metal hydrides and adsorbent packed bed, but no storage method has yet a clear technical and commercial future.

The storage in a solid-state matrix (e.g. metal hydride) has the advantage of being safe since chemisorption process makes in principle the pressure required to store a given amount of hydrogen much lower than what would be required if pure compression storage was used. Unfortunately, hydride based solutions result in quite heavy reservoir that do not fulfill the weight constraints related to mobile applications [2]. This shortcoming has motivated a large amount of work on lighter adsorbent materials, like Mg-based hydrides. Hydrogen physisorption has been also considered as one of the most promising storage methods for meeting the goals of the US Department of Energy (DoE) hydrogen plan for fuel cell powered vehicles [3,4].

Due to their microporous characteristics, low cost and accessibility at industrial level, microporous activated carbons appeared as a very good candidate for the development of porous packed bed hydrogen storage tank for mobile applications [5]. Zhou et al. [6] studied the hydrogen storage in AX-21

* Corresponding author: Laboratoire d'Ingénierie des Matériaux et des Hautes Pressions, CNRS UPR 1311-Université Paris 13, 93430 Villetaneuse, France. Fax: +33 1494 034 14.
E-mail address: hermosilla-lara@limhp.univ-paris13.fr
(G. Hermosilla-Lara).

Nomenclature

A	adsorption potential, $kJ\,mol^{-1}$
b	structural heterogeneity parameter
C_2	inertial resistance factor
E	characteristic energy of the adsorption system, $kJ\,mol^{-1}$
E_s	total energy of the solid phase, J
$\vec{F}$	force vector, N
h	species enthalpy, $J\,kg^{-1}$
$\vec{J}_i$	diffusion flux of species i, $kg\,m^{-2}\,s^{-1}$
Nl	volume expressed in liter under standard conditions
M_{H_2}	atomic mass of hydrogen, $kg\,mol^{-1}$
n	specific amount of adsorbed molecule, $mol\,kg^{-1}$
n_{lim}	highest adsorption that may be reached, $mol\,kg^{-1}$
n_0	specific amount of adsorbed molecules in the micropores at saturation, $mol\,kg^{-1}$
p	static pressure of the fluid, Pa
P_s	saturation pressure of gas, MPa
P_{lim}	limit pressure, MPa
R_1	internal diameter, m
R_2	external diameter, m
R_g	ideal gas constant, $J\,mol^{-1}\,K^{-1}$
S_h	source of heat, $W\,m^{-3}$

S_m	source of mass, $kg\,m^{-3}\,s^{-1}$
U	free-stream velocity, $m\,s^{-1}$
$\vec{v}$	overall velocity vector, $m\,s^{-1}$
v_i	velocity component along direction i, $m\,s^{-1}$

Greek letters

α	permeability, m^2
β	parameter of the modified DA model, $mol\,kg^{-1}\,K^{-1}$
γ	parameter of the modified DA model, $J\,mol\,K^{-1}$
$\dfrac{\partial n}{\partial t}$	kinetics of the adsorption reaction, $mol\,kg^{-1}\,s^{-1}$
ΔH	enthalpy of the adsorption reaction, $J\,mol^{-1}$
ε	porosity of the packed bed
ψ	parameter of the modified DA model, $mol\,kg^{-1}$
κ	parameter of the modified DA model, $kJ\,mol^{-1}$
λ_{eff}	effective conductivity of the packed bed, $W\,m^{-1}\,K^{-1}$
λ_f	thermal conductivity of the fluid, $W\,m^{-1}\,K^{-1}$
λ_s	thermal conductivity of the solid, $W\,m^{-1}\,K^{-1}$
μ	dynamic viscosity, Pa s
ρ_s	density of the solid phase, $kg\,m^{-3}$
ρ_g	density of the fluid phase, $kg\,m^{-3}$

activated carbon packed bed reservoir at liquid nitrogen temperature. They found, at a temperature of 77 K and a pressure of 6 Mpa, "gravimetric" and volumetric densities of 10.8 wt% and $41\,kg\,m^{-3}$, respectively. The "gravimetric" density value was, however, obtained without considering the weight of the reservoir envelope (only the weight of the packed bed was considered).

Unlike the chemisorption on metal hydrides where the absorption process involves a first step where the hydrogen molecule is dissociated and a second step where hydrogen atoms are linked to the metal by strong covalent bonds, adsorption on microporous carbon takes place through Van der Waals interaction between non-dissociated hydrogen molecules and active surface sites. But as these binding forces are weak, the physisorption process may be almost impeded by the Brownian motion if the temperature is too high. Actually, during the charging process of a packed bed reservoir, the exothermal adsorption phenomenon may lead to a significant temperature increase, which may result in a serious limitation of the packed material adsorption capacity and therefore in a limited storage performance of the considered tank. This issue is particularly severe for hydrogen as compared with other gases such as natural gas for which high energy storage performances can be readily achieved [7].

The main objective of this work is the investigation of thermal effects during high-pressure charging of the adsorbent packed bed reservoir. This paper is organized in five sections. The next section describes the experimental apparatus and the procedure

of charging the reservoir. Section 3 presents the mathematical model used to predict the time-variation of volume averaged temperature and pressure in the investigated tank. It also discusses the adsorption model used to describe the packed bed. In Section 4 the results obtained from both simulation and experiments are presented. Comparison between simulated and measured temperature histories are also used to understand the main phenomena that govern thermal effects during the tank charging phase. The main conclusions that may be drawn from this work are presented in the last section.

2. Experimental tests

2.1. Setup description

The experimental setup presented in Fig. 1 is composed of four parts: the storage tank, the charging circuit, the discharging circuit and the data acquisition system.

The storage tank is a cylindrical stainless-steel column, with internal (R_1) and external (R_2) diameters of 96 and 125 mm, respectively, and an internal length (L) of 255 mm. Six thermocouples are positioned along the column to obtain radial and axial temperature profiles. The base of the column is also equipped with a digital pressure transducer (DXD 1042 model, precision: $\pm 0.02\%$ of the full scale) manufactured by Heise, able to measure pressures up to 22 MPa. At the top of the column, the entry is sealed with an insulating tap. The column is packed with activated IRH3 carbon, which has an
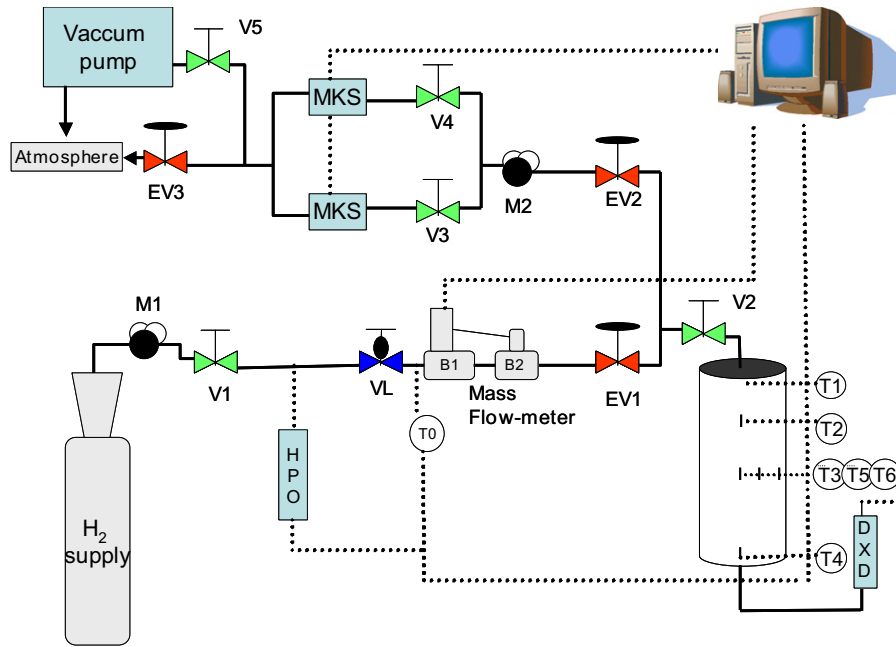
Fig. 1. Experimental setup for hydrogen storage.

measured average surface area of $2600 \, m^2 \, g^{-1}$ and a micropore volume of $1.6 \, ml \, g^{-1}$. The IRH3 activated carbon is produced from coconut coal by the Canadian *"Institut de Recherche sur l'Hydrogène"*.[1] The filling circuit is composed of a hydrogen bottle (internal pressure equal to 20 Mpa; purity: 99.99%) equipped with a pressure monitoring system which is linked through a pipe to the tank. The hydrogen flow is measured with a F-122M-FAB-88-V Bronkhorst mass flow-meter that allows to measure up to $100 \, Nl \, min^{-1}$ flow rate wit an accuracy of $\pm 1 \, Nl \, min^{-1}$. A regulation valve is coupled to this flow meter. The whole {flow-meter, regulation valve} system makes a possible to control and regulate the hydrogen flow entering the storage tank during the charging phase with a statistical reproducibility of $\pm 0.01\%$.

The micrometer valve (VL) (Fig. 1) is kept fully open during all the experiments, the beginning and the end of the charging process being monitored through a pneumatic valve ($EV1$). The flow rate is regulated through the regulation valve coupled with the flow meter.

The thermocouple positions are defined with respect to the tank inlet ($z = 0$) and to the tank axis ($r = 0$). Thermocouple $T1$ is located at the entry of the tank ($z = 0, r = 0$), $T2$ at ($z = L/4, r = 0$) and $T3$ at ($z = L/2, r = 0$). $T4$ is located in the vicinity of the tank bottom wall ($z = L - 5 \, mm, r = 0$), $T5$ is positioned off the symmetry axis at ($z = L/2, r = R_1/2$) and $T6$ is located at mid-height in the vicinity of the tank side wall ($z = L/2, r = R - 2 \, mm$).

Before each charging experiment, the gas present in the charging circuit is pumped out with a primary pump through a manual valve ($V5$).

The data acquisition system includes two multifunction boards (NI PCI-6014) linked to the thermocouples and flowmeters through two connecting interfaces (CB-68LP). The data were acquired by means of the Labview® (Labview 7.0) software. The acquisition frequencies for the temperatures and pressure are 6.25 and 1 Hz, respectively.

2.2. Experimental procedure

There are two key-parameters that characterize the tank charging phase. These are the charging pressure and the maximum admissible flow rate.

The tank charging experiments were carried out at a charging pressure of 10 Mpa. This pressure is set with the help of a high pressure manometer ($M1$) located between the hydrogen supply and the manual valve ($V1$). The charging pressure is the pressure that will be reached at the end of a charging experiment when the steady state situation is reached in the whole charging circuit including the storage tank.

The maximum admissible flow rate corresponds to the initial flow rate when tank charging is started. This is set with the help of the micrometer valve (VL). For this purpose a preliminary experiment is carried out with the tank isolated by closing the valve $V2$ and setting the charging circuit directly connected to the outlet through valve $EV2$, the manometer $M2$, the manual valve $V4$ and the electro-valve ($EV3$). During this preliminary experiment all the valves are first opened but the micrometer valve (VL). Then VL is progressively opened and the flow rate in the charging circuit measured. The micrometer valve position is set to the aperture leading to the desired value of the maximum admissible flow rate for the charging experiments. Since the pressure downwind the micrometer valve is set to a value of

1 MPa, the maximum admissible flow rate obtained in this way corresponds to a pressure drop almost equal to the charging pressure through the micrometer valve. It is worthy to mention at this stage that this maximum admissible flow rate is the maximum value that can be set for the charging flow rate. This would correspond to a situation where the regulation valve is fully open. Smaller initial flow rate may be obtained for the charging phase through a proper monitoring of the regulation valve (B2).

Once the charging pressure and the maximum admissible flow rate are set, the gas is pumped out from the charging circuit to reach a pressure of 50 mbars.

Then the charging circuit is isolated from the discharging circuit using the valve EV2. The valve EV1 is closed and the valve V1 is opened. Of course the aperture of the micrometer valve VL is set to a value corresponding to the maximum admissible flow rate and the regulation valve is dynamically monitored so as to yield the desired initial flow rate value.

The reservoir charging phase starts by opening the pneumatic valve EV1 (Fig. 1). It is ended by closing the same valve when the measured pressure reaches a steady state value that corresponds to the charging pressure. Of course, the flow rate goes to zero at the end of the charging stage when the pressures upstream and downstream the regulation valve are both equal to 10 Mpa.

During all this process the pressure at the bottom of the reservoir and the temperatures at the locations of the six thermocouples are recorded.

For each experiment, the external wall is kept in contact with the ambient atmosphere. This configuration may possibly lead to some variations of the heat transfer coefficient between the reservoir wall and the surrounding medium. Previous experiments on the same device showed however that the increase in the heat-transfer coefficient between the wall and the surrounding atmosphere by the use of a water jacket or by changing the wall material does not affect the maximum temperature within the bed, when an adsorbent bed with relatively low thermal conductivities is used [8]. This result is mainly due to the fact that the heat transfer from the reservoir to the surrounding atmosphere is limited by conduction fluxes in the packed bed.

3. Description of the numerical model

The main aim of the modeling study carried here is to analyze heat and mass transfer phenomena during hydrogen charging process and to help in the interpretation of the results that are obtained from the experiment described in the previous section. The numerical model used in this work is based on mass, momentum and energy conservation equations for flows in porous media. These equations are basically derived using volume averaging rules on a representative elementary volume. The details of a such derivation may be found in several books and papers (see [9] for example). We will restrict ourselves here on giving the main features of these equations. We will however focus on the mass and energy source terms due to adsorption phenomena since these terms give to the present study its main specificity.

It is worthy to mention here that since we are interested in the time-evolution of the temperature and the pressure, we consider the non stationary form of the conservation equations. We also make use of time-accurate algorithm to solve these equations.

3.1. The mass conservation equation

The time-dependent mass conservation equation for the hydrogen flow in an adsorbent porous bed may be written:

$$\frac{\partial \rho_g}{\partial t} + \vec{\nabla} \cdot (\rho_g \vec{v}) = S_m, \tag{1}$$

where ρ_g is the fluid density (kg m^{-3}), $\vec{v}$ is the overall velocity vector (m s^{-1}) and S_m is a mass source term or sink (kg m^{-3} s^{-1}).

The source term S_m accounts for the rate, in kg m^{-3} s^{-1}, of hydrogen transfer from gas phase to adsorbed phase. Assuming that the adsorption process is very fast, this rate may be derived on the basis of an equilibrium assumption using the following equation:

$$S_m = -M_{H_2} \rho_s \frac{(1-\varepsilon)}{\varepsilon} \frac{\partial n}{\partial t}, \tag{2}$$

where M_{H_2} is the atomic mass of hydrogen and ε is the porosity of the packed bed, ρ_s the density of the solid phase (kg m^{-3}) and $\partial n / \partial t$ the kinetics of the adsorption reaction (mol kg^{-1} s^{-1}).

3.2. The momentum equation

Neglecting the momentum loss due to adsorption phenomena, the time-dependent momentum transport equation is similar to the one used for classical homogenous porous media. It may be written:

$$\frac{\partial}{\partial t}(\rho_g v_i) + \nabla \cdot (\rho_g \vec{v} v_i) = -\frac{\partial p}{\partial x_i} + [\nabla \cdot (\bar{\bar{\tau}})]_i + F_i, \tag{3}$$

where ρ_g is the fluid density, p the static pressure, $\vec{v}$ is the overall velocity vector (m s^{-1}), v_i the component of the velocity along the direction i, $\bar{\bar{\tau}}$ is the stress tensor, and $\vec{F}$ represents an additional friction term due to the porous medium.

The friction source term accounts for the interactions between the flowing gas and the solid porous medium. These interactions include a local viscous dissipation at the pore scale and an inertial force due to the strong geometrical variation of the flow lines at the pore scale. These are accounted for with the expression:

$$\vec{F} = -\left(\frac{\mu}{\alpha}\vec{v} + C_2 |\vec{v}|\vec{v}\right), \tag{4}$$

where μ is the viscosity, α is the permeability and C_2 is the inertial resistance factor.

3.3. The energy balance

The energy balance equation is similar to those classically used to describe flows in porous media. It includes however

a source term S_h that accounts for the energy release during adsorption process. The equation may be written:

$$\frac{\partial}{\partial t}(\varepsilon \rho_g E_g + (1-\varepsilon)\rho_s E_s) + \nabla \cdot (\vec{v}(\rho_g E_g + p))$$
$$= \nabla \cdot ((\lambda_{\text{eff}} \nabla T) + (\bar{\bar{\tau}} \cdot \vec{v})) + S_h, \qquad (5)$$

where ε is the porosity of the packed bed, ρ_g is the fluid density, ρ_s the solid density, E_g the total energy of the fluid, E_s the total energy of the solid powder, $\vec{v}$ is the overall velocity vector, p the static pressure of the fluid, and λ_{eff} is the effective thermal conductivity of the medium.

$$S_h = \Delta H \cdot S_m, \qquad (6)$$

where ΔH is the enthalpy of the adsorption reaction.

The effective thermal conductivity of the porous media, λ_{eff}, is defined as the volume average conductivity of the porous medium taking into account the presence of the solid and gas phase. It may be therefore expressed as function of the solid and gas conductivities and the porosity, i.e.:

$$\lambda_{\text{eff}} = \varepsilon \lambda_f + (1-\varepsilon)\lambda_s, \qquad (7)$$

where λ_f represents the thermal conductivity of the fluid and λ_s the thermal conductivity of the solid powder.

3.4. Adsorption model

Several existing models have been investigated in order to develop an equation describing the adsorption isotherm over wide ranges of temperature and pressure. The most widely used models are: (i) the Virial equation which permits to determine the isosteric heats at zero coverage [10,11], and (ii) the Dubinin–Astakhov (D–A) equation that makes use of volume filling of micropores (TVFM) concept and some structural or energetic parameters derived from best fits with measured isotherms [12]. The D–A model enables to build up practically useful classifications of different adsorbent materials. The use of the very first version of D–A equation is however possible only if the working pressure is below the saturation pressure. Consequently, this first version of D–A model cannot be used under supercritical conditions since in this condition condensation phenomenon does not take place and saturation pressure has no physical meaning [13]. Despite this shortcoming, some authors tried to extend the D–A model to the supercritical conditions by assuming that the adsorbate phase may be described as a "overheated liquid" [14] or "quasi-liquid" state [15].

The D–A equation may be written as follows:

$$n = n_0 \exp\left[-\left(\frac{A}{E}\right)^b\right], \qquad (8)$$

with n the specific amount of adsorbed molecule (mol kg^{-1}), n_0 the specific amount of adsorbed molecules in the micropores at saturation (mol kg^{-1}), A is the adsorption potential (kJ mol^{-1}), E is the characteristic energy of the adsorption system (kJ mol^{-1}), and b is the structural heterogeneity parameter.

The adsorption potential A is defined as

$$A = R_g T \ln \frac{P_s}{P}, \qquad (9)$$

where P_s is the vapor saturation pressure (the equilibrium pressure at the gas–liquid phase transition).

As discussed previously, the vapor saturation pressure P_s of hydrogen does not exist when equilibrium temperature is above its critical temperature T_C (33.2 K in the case of H_2). In this case the parameters (n_0, E, b) of the D–A equation should be modified, since the adsorption mechanisms do not follow the TVFM. High-pressure adsorption under supercritical conditions indeed involves the formation of several layers, while the D–A model assumes that the adsorption involves only one monolayer [16]. In addition, mesopores and even macropores could participate to the adsorption at high pressure. This will also favor a multi-layer adsorption mechanism. Consequently, the specific amount of saturated adsorbed molecules in the micropores n_0 and the characteristic energy E of the adsorption system will depend on the equilibrium temperature at high pressure. In principle, the parameter b would also vary with pressure and temperature. We followed however the approach of Zhan et al. [17] and have chosen $b = 2$ which is consistent with the original Dubinin–Raduskevich model. These authors described the variation of n_0 and E by using the following expressions:

$$n_0 = f(T) = \psi + \beta T, \qquad (10)$$

$$E = g(T) = \kappa + \gamma T. \qquad (11)$$

They also used the concept of limit pressure P_{lim}, as suggested by Zhou and Zhou [13] who considered that there is a pressure above which the adsorption capacity of the considered material decreases. They used this pressure limit defined as P_{lim} instead of the saturation pressure to describe adsorption with D–A model under supercritical conditions. To this pressure limit corresponds an adsorption limit n_{lim} which represents the highest adsorption that may be reached for the considered material. They therefore end up with the following modified adsorption potential:

$$A = R_g T \ln \frac{P_{\text{lim}}}{P}. \qquad (12)$$

The procedure proposed by Zhan et al. [18] which is summarized above was applied to the present work to describe the adsorption isotherms of the considered IRH3 activated carbon. The values of ψ, β, γ and κ necessary to estimate n_0 and E were obtained from a best fit with the experimental isotherms (Fig. 2). They are listed in Table 1. The value of P_{lim} was also determined from the experimental measurements.

The wall temperature is assumed constant in the numerical model since the total energy released by the charging phenomenon would increase the temperature of the total mass of steel of about 2 K only, which is negligible. The inlet boundary condition consists of a prescribed mass flux. The chosen grid contains 2100 cells the grid meshes were refined near the walls and the symmetry axis.
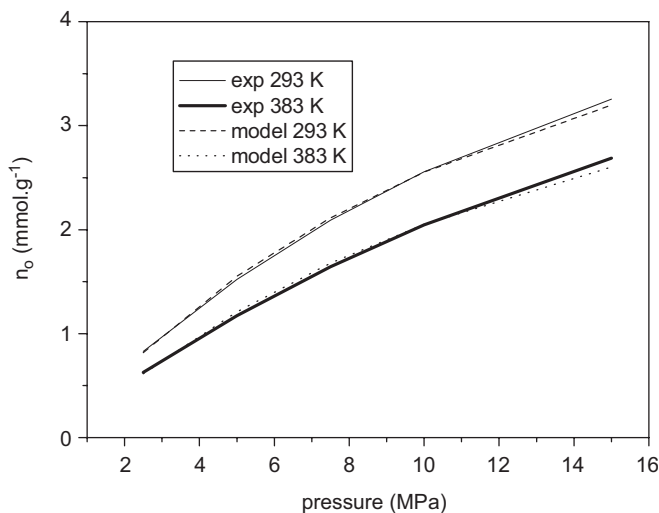
Fig. 2. Hydrogen adsorption isotherms: experiments vs. model.

Table 1
Value of the constants introduced in our model

$P_{\lim}$(MPa)	ψ (mmol g^{-1})	β (mol kg^{-1} K^{-1})	κ (kJ mol^{-1})	γ (J mol K^{-1})
77.75	7.3235	-0.0088	772.92	18.828

4. Results and discussion

4.1. Experimental results

We first investigated the changes in the charging phase duration and the temperature value at the hottest position in the tank with the initial inlet flow rate. The porous storage tank was fed with hydrogen in these first experiments.

Fig. 3 shows the time-variation of the flow rate for different value of initial flow rate. One may distinguish two main regions. The first one corresponds to a constant flow rate that corresponds to the value prescribed with the help of the regulation system composed of the mass flow-meter and the regulation valve. Then, we have a second fairly short phase where the flow decreases very rapidly to zero. During this second phase the pressure drop through the regulation valve is so small that the flow rate is smaller than the prescribed value even though the regulation valve is fully open. The flow is therefore fully determined by the pressure drops through the different components of the charging circuit (valves, flow-meter and so,…). It therefore decreases with the pressure drops through the components of the charging circuit until an equilibrium situation is reached and the pressure is constant over all the charging circuit and the storage tank.

Fig. 4 shows the measured time-variations of the temperature at different radial and axial positions in the bed during hydrogen charging. We note that the larger temperature values are recorded on $T3$ which is located at the mid-height and on the axis of the tank (Fig. 4a and b). This could be expected since the wall effect is smaller at this location and $T3$ is not subject to thermal cooling through fresh hydrogen convective

flow as would be the case for $T1$ which is located at the tank inlet. The temperature near the bottom wall of the tank ($T4$) is higher than that measured near the side wall ($T6$). This is probably due to the fact that the bottom wall receive an extra convective flow of hot hydrogen coming from the internal hot region of the tank ($T3$ region). This is not the case of the lateral wall where the main energy flux is due to conduction.

Fig. 5 shows the effect of the initial flow rate on the charging time. The way how the charging time is estimated is also indicated on the figure. The filling time is the abscissa of the intersection point between the line tangent to the pressure time variation curve at $t = 0$ and the horizontal pressure line corresponding to the final state. Basically, the charging time varies linearly with the inverse of the initial flow rate. In other words, when the initial flow rate is increased by a factor around 2 the charging time is reduced by the same factor. This shows that the contribution of the gas fed during the second phase of the charging process when the flow rate decreases is negligible, and almost all the gas is fed during the first charging phase when the flow rate can be considered as constant. Consequently, the flow rate in the experiments discussed may be considered as nearly constant.

The maximum temperature value reached in the hottest region of the reservoir is around 340 K for a flow rate of 9.5×10^{-4} Nm^3 s^{-1}. This value decreases only slightly when the flow rate is decreased by a factor 2. A difference of less than 8 K is indeed obtained between the maximum temperature values recorded on $T3$ with flow rates of 5×10^{-4} and 9.5×10^{-4} Nm^3 s^{-1} (Fig. 6). Also of interest the fact that the maximum temperature is reached at a time corresponding to the end of the charging process (Fig. 6).

The rate of temperature increase is therefore much higher when a larger flow rate is used. The very weak dependence of the temperature value at the tank inlet on the flow rate is essentially due to the poor thermal conductivity of the adsorbent bed (0.2 W m^{-1} K^{-1}). The heat transfer to the reservoir wall exhibits very long characteristic time, i.e. about 2000 s. This characteristic time which corresponds to the time needed to reach the thermal equilibrium inside the tank was determined experimentally. However, to make the heating effect that takes place during 200 s clearly visible in Fig. 4b, the decrease of the temperature down to the wall temperature value was not reported in Fig. 4b. The characteristic time cannot be deduced from this figure. The rate of the temperature increase only depends on the charging flow rate. On the other hand, the maximum temperature would depend on the total amount of the energy released by adsorption process, on the mechanical dissipation that comes with the charging process and on the energy loss through energy transfer to the wall. Since the amount of hydrogen adsorbed in the two experiments is almost the same, the energy released by adsorption is also almost the same. The energy transfer through conduction to the wall takes place over very long time and is very weak during the charging phase. The heat release due to the dissipation of the mechanical energy of the feed gas is, however, slightly less important in the case of smaller flow rate. This may explain at least partly the slightly smaller maximum value of the temperature obtained for longer
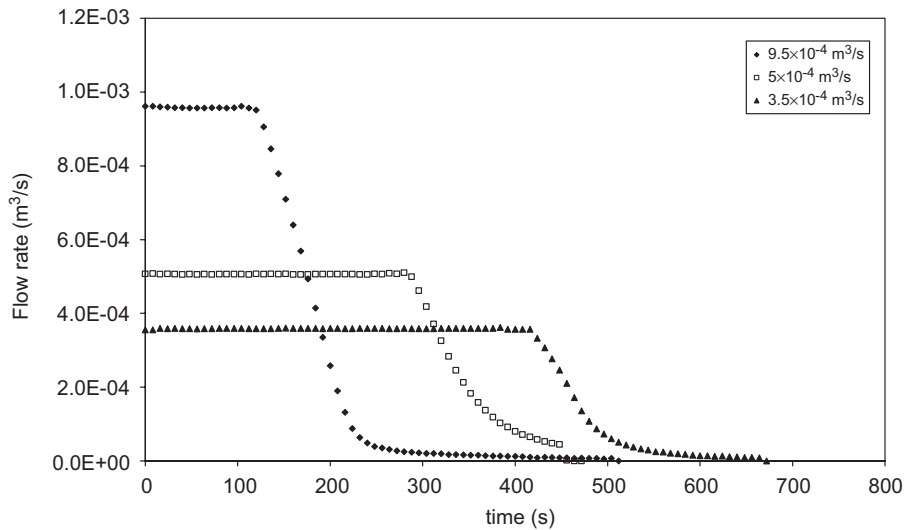
Fig. 3. Typical flow rate profiles at different regulation values with hydrogen.
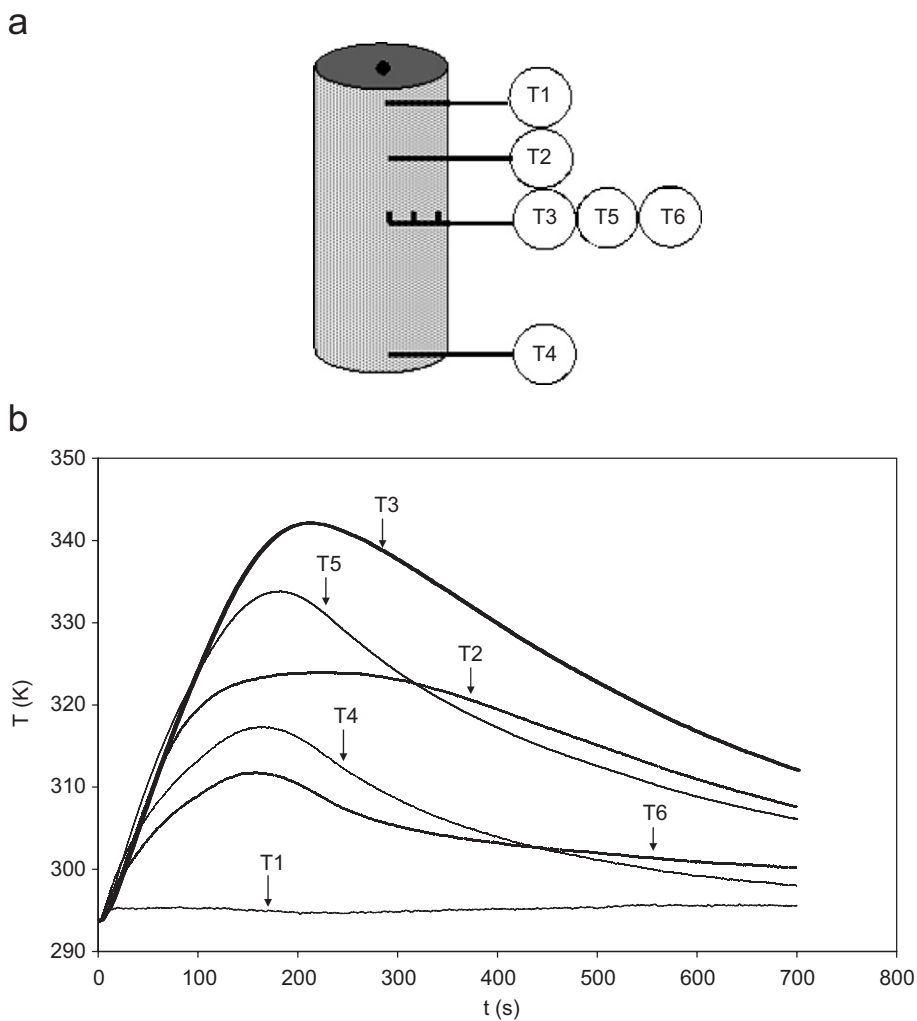

Fig. 4. (a) Sketch of the reservoir showing the locations where these temperatures are recorded. (b) Experimental temperature histories at various positions in the tank for a charge pressure of 10 MPa and with a flow rate regulated at $9.5 \times 10^{-4}\,\mathrm{m}^3\,\mathrm{s}^{-1}$ of hydrogen.
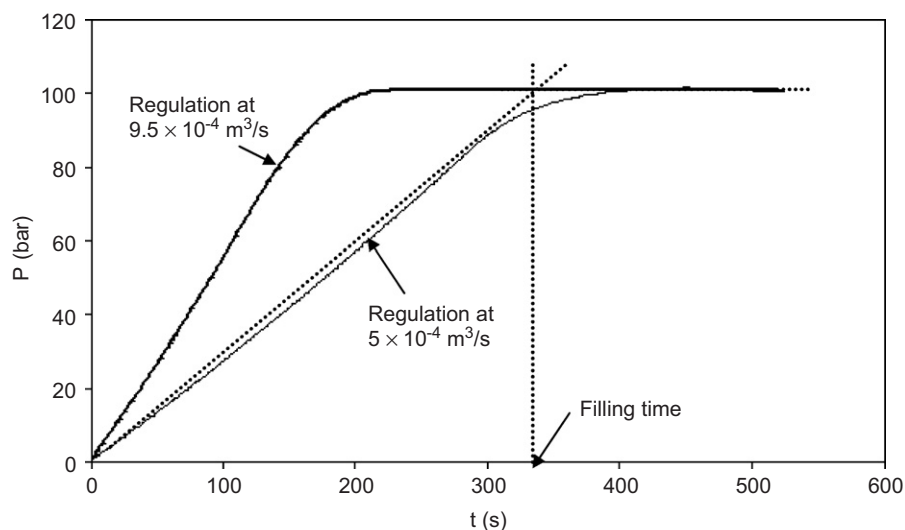
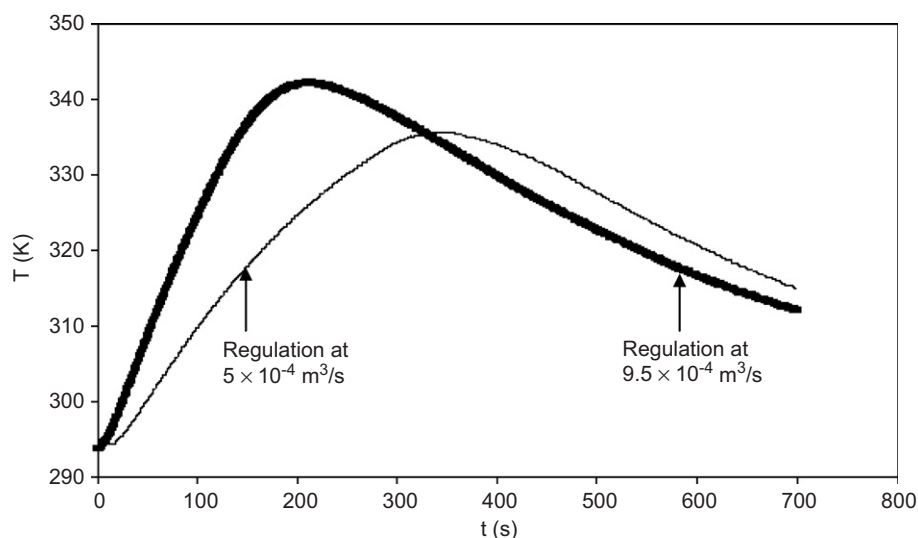Fig. 5. Experimental pressure profiles for two different initial flow rates of hydrogen.

Fig. 6. Effect of the initial flow rate on the experimental temperature evolution at the hottest location ($T3$) for the case of hydrogen.

heating dynamic, i.e., smaller flow rates. The temperature increase is due to two phenomena: (i) the exothermic process of adsorption on one hand, and (ii) the heat released through the dissipation of the mechanical energy of the feed gas, on the other hand.

To estimate the respective weights of these two different energy dissipation routes, we carried out additional tank charging experiments with helium as the charging gas. Since the adsorption of helium on activated carbon is negligible [19], the temperature increase observed with helium would be mainly due to the thermal dissipation of the mechanical energy of the feed gas. Two experiments using hydrogen and helium as a feed gas were therefore carried out with the same charging pressure, 10 MPa, and initial flow rate, 3.53×10^{-4} Nm^3 s^{-1}.

Fig. 8 shows the time-variations of the temperature in the hottest region of the tank when helium and hydrogen, are, respectively, used as feed gas. The maximum temperature

obtained for hydrogen is significantly higher than that obtained for helium with a difference of 7 K, which represents almost 22% of the total temperature increase.

Table 2 reports the total injected gas volume, the temperature increase in the hottest region and the filling time for the two experiments. It is interesting to note that the filling time with H$_2$ as a feed gas is 210 s longer than when helium is used as feed gas. If we assume that no adsorption occurs with helium the additional gas volume injected in the case of hydrogen would correspond to the gas that is adsorbed in the activated carbon porous bed. This would correspond to 21.6 Nl of hydrogen, which represents almost 15% of the hydrogen stored as compressed gas in the tank filled with the packed bed.

Knowing that the tank is filled with 440 g of IRH3 AC, the present experiment allows a rough estimation of the adsorption capacity of the used activated carbon. A value of 0.44 wt% was estimated, which is not far from the value obtained with the

Table 2
Comparison of the filling values for H$_2$ and He charging cases

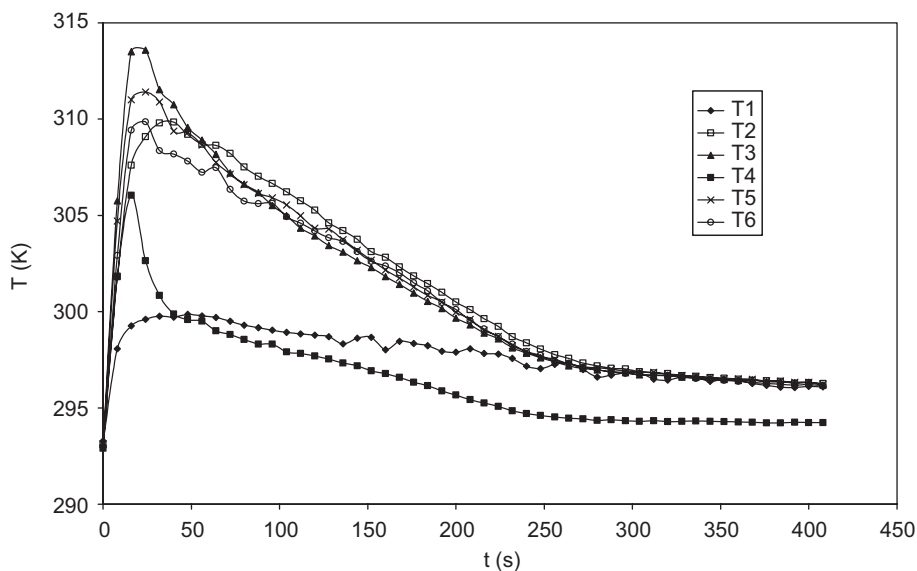|	End pressure (bar)	Injected total volume of gas (l)	ΔT at the hottest location (K)	Filling time (s)
Filling with H$_2$	100.5	169.5	37.6	470
Filling with He	99.8	147.9	30.8	260

Fig. 7. Temperature histories without adsorbent material (empty tank) for a charge pressure of 10 MPa and with a flow rate regulated at $9.5 \times 10^{-4}\,\mathrm{m^3\,s^{-1}}$.

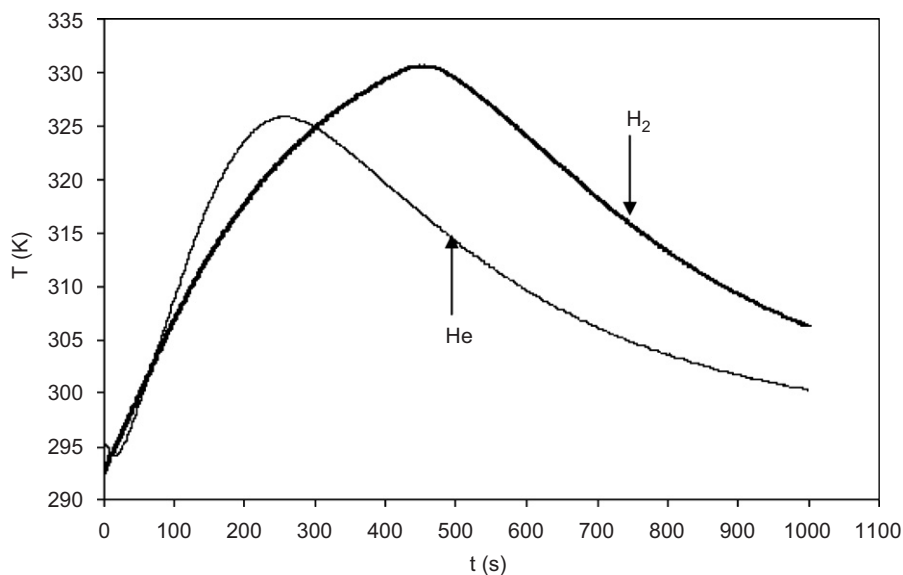
Fig. 8. Comparison of the experimental temperature evolution at the hottest location ($T3$) obtained with hydrogen and helium charging with an initial flow rate regulated at $3.53 \times 10^{-4}\,\mathrm{m^3\,s^{-1}}$.

more accurately determined adsorption isotherm, i.e., 0.5 wt% at 298 K and 10 MPa. This difference is due to the fact that our experiment is not well designed to accurately determine adsorption capacity isotherm (with an accuracy less than 5%).

Table 2 shows that for the investigated IRH3 AC, 78% of the energy release that accompany the charging process is due to the dissipation of the mechanical energy of the feed gas. The remaining 22% of this temperature increase comes from

hydrogen adsorption process. Of course more effective adsorbent materials would lead to much stronger temperature increase with a larger contribution of the adsorption phenomenon.

To show the effect of the porous bed on the heating dynamics in the tank we performed an experiment with an empty tank. Fig. 7 shows the temperature histories obtained in such a configuration. The heating dynamics is much faster than when a packed bed is used. The maximum values of the temperature are reached only few seconds after the charging phase starts, and the temperature increase is much lower than that observed in the presence of packed bed. After the heating phase a temperature decrease takes place and the equilibrium situation is reached in mush smaller time than those obtained when the tank filled with an activated carbon. This means that the convective transfer is significant and insures rapid thermal dynamics in the case of empty tanks (Fig. 8).

4.2. Simulations with fluent software

Fig. 9 shows the 2D axisymmetrical geometry used for the simulations of the charging of the reservoir. The wall tempera-
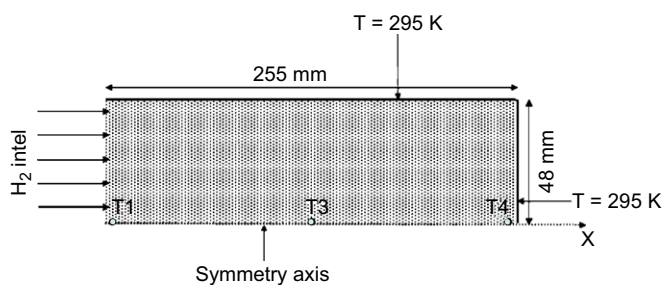
ture is kept constant during all the charging phase since the total energy released by the charging phenomenon would increase the temperature of the steel made wall by no more than 2 K. The temperature inside the packed bed is recorded at three different locations where experimental measurements were also performed.

The actual storage tank is fed through a small 2 mm diameter aperture which suddenly enlarges in the whole 100 mm diameter cylindrical tank. Taking into account this configuration would make the computation more complex and is in fact not necessary. The flow in a packed bed is indeed mainly governed by the product of the Reynolds number (Re) and the Darcy number (Da), $ReDa$. It was shown[2] that the velocity profile of gas jet entering a large reservoir through very small aperture tends to flatten and behave as a plug flow after a distance negligible with respect to the tank diameter when the product $Re \times Da$ is below 2×10^{-5}. In the situation investigated here this distance is less than 5% of the tank height. Since the condition $Re \times Da < 2 \times 10^{-5}$ is fulfilled in the investigated configuration, the simulation domain is chosen so as the axial velocity of the gas flow may be considered as radially constant at the inlet of the simulation domain. This does not include the region where the flow expands from the small aperture to the whole tank. It does neither include the bed region where the flow is not homogenized. A flat velocity profile corresponding to an initial mass flow rate of 10^{-4} kg s^{-1} is specified as a boundary condition at the simulation domain inlet. The time evolution of this flow rate is described by a sixth order polynomial fit to the experimental flow rate.

It is worthy to mention again at this stage that the simulation domain is located far downwind the expansion micrometer valve. Anticipating on the results, the flow in the simulation domain is basically isobaric, the spatial variation of the

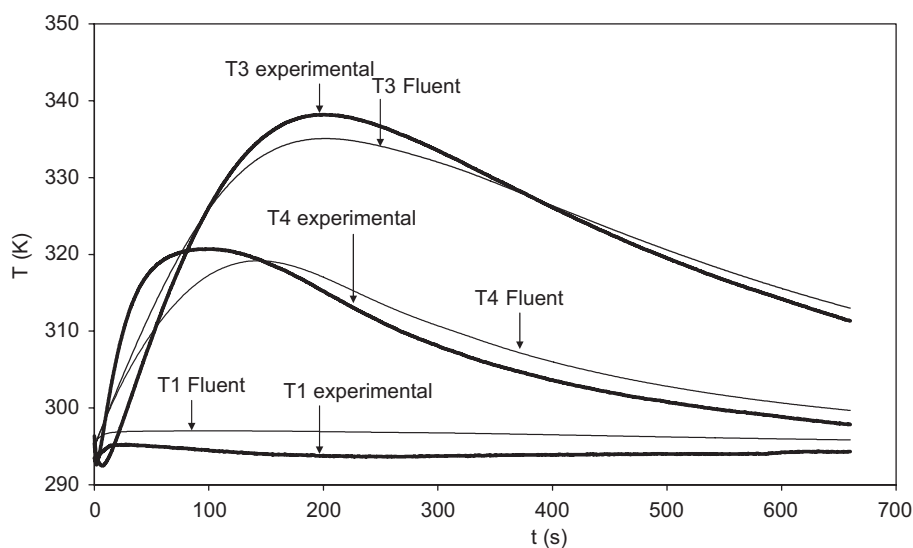Fig. 9. Sketch of the simulated tank showing the boundary conditions.

Fig. 10. Comparison of the experimental and numerical temperature profiles at different locations in the tank for an initial flow rate equal to 9.5×10^{-4} m^3 s^{-1} and a final pressure of 10 Mpa.

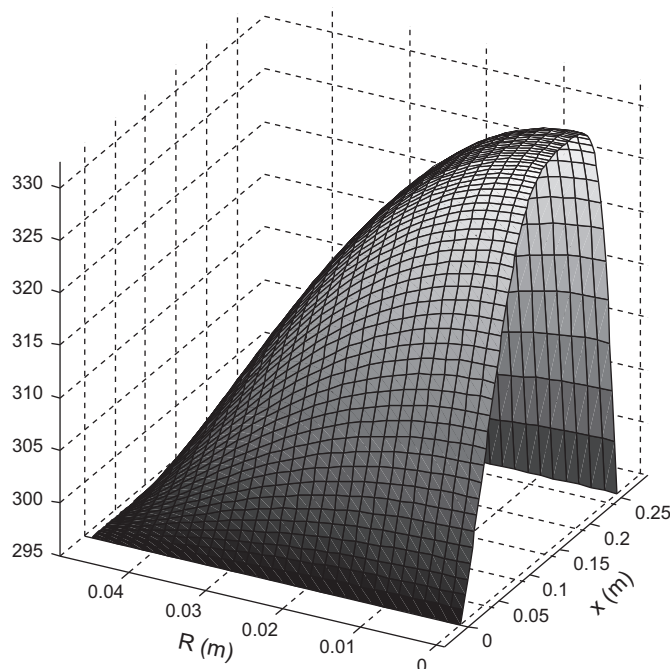[2] Final report of the H2THERM project (September 2005).

Fig. 11. Surface of hydrogen temperature in the tank at time $t = 360$ s.

pressure is negligible with respect to its spatially averaged value. The tank charging proceeds therefore through a successive quasi-isobaric configurations with a pressure that increases with time. It was therefore not necessary to include any Joule–Thomson effect in the simulation.

The bed is represented as a one scale porosity medium. The porosity was chosen equal to 0.88.

Fig. 10 shows the comparison of the experimental and numerical temperature profiles at different locations. The inlet temperature is almost constant during all the charging phase, while the hottest zone is located at the same coordinate as those determined experimentally, i.e. at the center of the tank. The same amplitude of temperature increase is obtained at the different locations. The times where the peaks appear are about equal at a considered location which means that the flow dynamics is well depicted by the model.

Fig. 11 shows the temperature distribution of hydrogen in the tank. The maximum temperature zone is not centered but a little shifted down to the bottom because of the flow effects. The temperature gradients lead to density variations between 6.61 and $7.45\,\text{kg}\,\text{m}^{-3}$. The highest density is obtained near the wall where the temperature is the lowest, while the lowest densities are obtained in the hottest region.

5. Conclusion

The temperature and pressure dynamics during the charging process of an IRH3 packed bed storage tank were experimentally and numerically investigated. Experiments carried out in similar conditions on hydrogen and helium showed that the adsorption process contributes to less than 22% of the

observed heating effects. The maximum temperature achieved in the packed bed is mainly governed by the amount of hydrogen charged in the reservoir and the adsorption capacity and enthalpy of the adsorbent. The dynamic of the temperature increase is governed by the hydrogen inlet flow rate.

The commercial code fluent seems suitable for the simulation of the charging phase in a packed bed storage tank. Its predictions of the temperature or pressure increases are in fair agreement with the experimental measurements and we consider using this tool to design a future industrial heat exchanger.

Experiments with more efficient activated carbons are however necessary to get more accurate evaluations of the adsorption contribution to the temperature increase in situation of practical interest. Experiment at higher pressure would be also of interest, since they would lead to a stronger heating. Improvement of the thermal transfer between the bulk of the reservoir and outside walls would be also interesting to investigate for limiting the heating phenomenon. This can be made by inserting supplementary interbed heat exchangers, such as fins, to the system.

This study was carried out on the presently available activated carbon. The methodology used may be however applied to materials with higher adsorption capacity and strong potential for mobile applications. The same methodology may be also applied to investigate the thermal effects under cryogenic conditions at which the adsorption capacity of the available material is high enough to make them interesting for mobile applications.

References

[1] De Luchi. Hydrogen fuel cell vehicles. University of California at Davis: Institute of Transportation Studies; 1992.

[2] Zhou L. Progress and problems in hydrogen storage methods. Renewable Sustainable Energy Rev 2005;9:395–408.

[3] Hynek S, Fuller W, Bentley J. Hydrogen storage by carbon sorption. Int J Hydrogen Energy 1997;22(6):601–10.

[4] Dillion AC, Jones KM, Bekkedahl TA, Kiang CH, Bethune DS, Heben MJ. Storage of hydrogen in single-walled carbon nanotubes. Nature 1997;386:377.

[5] Zhou L, Zhou Y, Sun Y. A comparative study of hydrogen adsorption on superactivated carbon versus carbon nanotubes. Int J Hydrogen Energy 2004;29:475–9.

[6] Zhou L, Zhou Y, Sun Y. Enhanced storage of hydrogen at the temperature of liquid nitrogen. Int J Hydrogen Energy 2004;29:319–22.

[7] Corless J, Barclay JA. In: Kittel, P. editor. The effects of refueling system operating pressure on LNG and CNG economics. Adv Cryogenic Eng 1995;41b:1033–40.

[8] Delahaye A, Aoufi A, Gicquel A. Improvement of hydrogen storage by adsorption using 2D modeling of heat effects. AIChE J. 2002;48(9):2061–73.

[9] Bejan A, Nield DA. Convection in porous media. 2nd ed., Berlin: Springer; 1999.

[10] Ross S, Olivier JP. On physical adsorption. New York: Interscience; 1964.

[11] Czepirski L, Jagiello J. Virial-type thermal equation of gas–solid adsorption. Chem Eng Sci 1989;44(4):797–801.

[12] Dubinin MM. In: Cadenhead DA, editor. Progress in membrane and surface science, vol. 9. New York: Academic Press; 1975 (chapter 1).

[13] Zhou L, Zhou Y. Linearization of adsorption isotherms for high-pressure applications. Chem. Eng. Sci. 1998;53(14):2531–6.

[14] Ozawa S, Kusumi S, Ogino YJ. Physical adsorption of gases at high pressure IV An improvement of the Dubinin–Astakhov adsorption equation. J Colloid Interface Sci 1976;56(1):83–91.

[15] Kaneko K, Shimizu K, Suzuki TJ. lntrapore field-dependent micropore filling of supercritical N_2 in slit-shaped micropores. Chem Phys 1992;97(11):8705–11.

[16] Amankwwah KAG, Schwarz JA. A modified approach for estimating pseudovapor pressures in the application of the Dubinin–Astakhov equation. Carbon 1995;33(9):1313–9.

[17] Zhan L. et al. A linear comprehensive adsorption model of hydrogen on super activated carbon under supercritical conditions. J Colloid Interface Sci 2002;250:63–6.

[18] Zhan L, Li KX, Zhang R. Improvements of the DA equation for application in hydrogen adsorption at supercritical conditions. J supercritical fluids 2004;28:37–45.

[19] Bae J-S, Do DD. Surface diffusion of strongly adsorbing vapors in activated carbon by a differential permeation method. Chem Eng Sci 2003;58(19):4403–15.